Available online at www.sciencedirect.com

Manufacturing Letters

Manufacturing Letters 35 (2023) 468–476

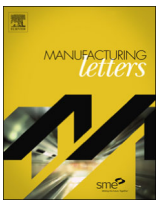

51st SME North American Manufacturing Research Conference (NAMRC 51, 2023)

Modulated Orthogonal Cutting System Realized by Piezo Stack Actuation and Linear Guide Coupling

Aaqib Ali[a], Jianxin Zhao[a], Patrick Kwon[a], Burak Sencer[b], Yang Guo[a,*]

[a]*Department of Mechanical Engineering, Michigan State University, East Lansing, 48824, MI, USA*
[b]*School of Mechanical, Industrial and Manufacturing Engineering, Oregon State University, Corvallis, 97331, OR, USA*

Abstract

Modulation-assisted machining (MAM) employs low-frequency feed-direction tool vibration to enhance conventionally continuous cutting processes such as turning, drilling, and boring operations. The development of a suitable tool vibration system is critical for the success of MAM. In this paper, a tool vibration system realized by using piezo stack actuation and linear guide coupling was designed and constructed. The performance of the system was evaluated by conducting orthogonal tube face turning tests on AISI 1045 steel using a range of cutting and modulation conditions. Cutting forces and tool vibration displacement were measured and analyzed. A mechanistic force model based on the variable uncut chip thickness was used to predict the variable primary cutting and feed forces in MAM which showed good agreement with the measured forces. Furthermore, It was found that the vibration amplitude with cutting was reduced when compared to the vibration amplitude without cutting. The reduction in vibration amplitude was predictable as it depends on the feed force and the stiffness of the system. The results indicate good control ability of the tool vibration system across a wide range of cutting and modulation conditions.

Keywords: feed modulation; tool vibration; orthogonal cutting; piezo stack actuation.

1. Introduction

Modulation-assisted machining (MAM) is a novel machining process in which a controlled low-frequency (typically less than 300 Hz) tool vibration is applied in the tool feed direction to enable periodic tool-chip and tool-work disengagements during the cutting process. MAM can transform a conventional continuous cutting process, such as turning, boring, or drilling, into a discrete cutting process. There are many benefits resulting from MAM. Firstly, chip breaking is guaranteed which leads to better chip management. This is particularly useful for improving chip ejection in deep hole drilling applications [1][2]. Secondly, the cutting tool can be better cooled and lubricated due to the periodic tool-chip disengagements [3]. This is particularly useful for reducing the tool wear and increasing the tool life for machining difficult-to-cut materials. For instance, it has been shown that MAM increases the tool life of cubic boron nitride (CBN) tools at least 20 times when turning compacted graphite iron (CGI) at a high speed of 730 m/min compared to conventional machining (CM) [4]. Thirdly, the controlled low-frequency tool vibration can suppress the high-frequency self-excited chatter vibration leading to the improved dynamic stability of the cutting process [5][6]. Therefore, a higher material removal rate can be achieved by MAM.

The development of a suitable tool vibration system is critical for the application of MAM. For MAM drilling, a range of methods has been used to realize the feed-direction vibration of the drill tool. These methods include linear motor drives [7][8], electromagnetic shakers [9], self-excited vibrating structure [10], bearings with wavy race surfaces [11], and piezoelectric actuators [12].

For MAM turning, two general methods have been utilized. The first method is to directly control the CNC machine slide

* Corresponding author. Tel.: +1-517-432-3164.
E-mail address: yguo@msu.edu (Yang Guo).

Nomenclature

A	modulation amplitude (mm)
h_0	feed per revolution (mm/rev)
ϕ	phase shift of tool path between successive spindle revolutions (radians)
f_m	modulation frequency (Hz)
f_w	workpiece rotation frequency (Hz)
v_c	cutting speed (m/min)
h	uncut chip thickness (mm)
b	width of cut (mm)
A_{pp}	peak-to-peak modulation amplitude (mm)
V_{pp}	peak-to-peak applied voltage amplitude (V)
F_c	primary cutting force (N)
F_f	feed force (N)

to realize the modulation of the feed motion. The benefit is that there is no need to attach additional tool vibration equipment to the machine. For a common CNC machine, this can be achieved by special CNC programming. This has been termed as modulated tool path (MTP) technology [13]. However, due to the large vibrating mass (machine slide) involved, the modulation frequency which can be achieved is typically low (< 20 Hz). Citizen Machinery in Japan has produced a special CNC Swiss machine that can perform both turning and drilling with feed motion modulation by controlling the X-axis and Z-axis motions. It has been termed alternatively as low-frequency vibration (LFV) machining [14]. The modulation in Z-axis is realized by the work holding spindle while the X-axis modulation is realized by the linear drive of the slide. It has been claimed that the maximum modulation frequency that can be realized is ~100 Hz. The Swiss machine is only used for machining small-diameter parts (e.g., bone screws, etc.). This is why the Z-axis modulation can be realized by vibrating the workpiece. However, this method imposes limitations on the size of the workpiece.

The second method is to utilize piezo stack actuation to realize feed-direction tool vibration. This method requires installing additional equipment onto a CNC machine, but with proper design, the vibrating mass can be minimized. This allows more precise control of the vibration condition (frequency and amplitude), and a wider range of vibration conditions can be achieved. The main design challenge is how to couple the piezo stack actuator with the tool holding structure such that the feed direction tool vibration can be actuated by the piezo stack while tool motion in the cutting and radial directions can be constrained. One way is to utilize a flexural hinge structure [15][16]. This design is limited by the flexure hinges because the modulation frequency can be affected if the flexure hinges deform too much. Therefore, the allowable modulation frequency and feed rate are restricted due to hinge design. The other way is to utilize a linear guide coupled with the piezo stack actuator [17]. This is essentially to create an additional small slide on the machine which will be driven only by the piezo stack actuator. Since various types of linear guides are commercially available, the design and construction of a piezo stack actuated tool vibration system can be simplified.

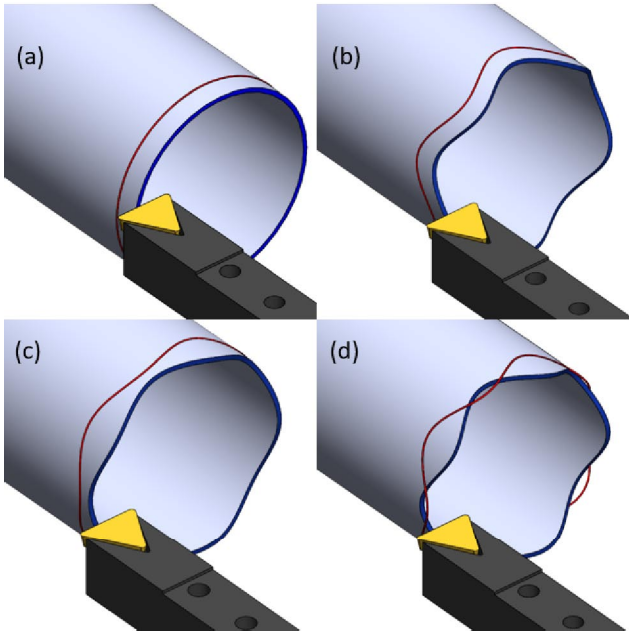

Fig. 1: Schematic of orthogonal tube turning under a) CM, b) in-phase MAM, c) out-of-phase MAM with insufficient amplitude, and d) out-of-phase MAM with sufficient amplitude.

Previous studies have been mainly focused on the kinematics [18], mechanics [13][15], and dynamics of the MAM process [5]. Additionally, investigations have explored the impact of MAM on tool life [17] and surface finish [16]. In these studies, either the cutting conditions (speed, feed, and depth of cut) or the modulation conditions (frequency and amplitude) that can be tested are often restricted by the employed modulation equipment and system. However, there have not been many reported studies on evaluating the performance and limitations of the modulation equipment. Such a study is important as the performance of the modulation system is critical to the success of MAM process. In this study, a simple modulation system realized by coupling a piezo stack actuator and a linear guide is experimentally evaluated by conducting orthogonal tube turning tests on AISI 1045 steel. The results show good control ability of the modulation system across a wide range of cutting and modulation conditions.

2. Kinematics of Modulation-Assisted Machining

To achieve effective MAM, the modulation frequency and amplitude need to be properly controlled for the given cutting conditions. This can be guided by the kinematic model of MAM which is briefly reviewed here. Figure 1 illustrates the cutting kinematics of MAM using the orthogonal tube turning configuration. For conventional machining (CM) (Fig. 1a), the constant feed rate generates a parallel helical tool path on the rotating tube-shaped workpiece. The tool path does not intercept be-

tween successive workpiece revolutions, so the tool is always engaged with the workpiece producing continuous chips with constant uncut chip thickness. The constant tool feed rate can be modulated by superimposing a tool vibration in the feed direction to generate a wavy tool path with respect to the workpiece. If the wavy tool path between successive workpiece revolutions is in phase (Fig. 1b), the tool will still be always engaged with the workpiece producing a continuous chip with constant uncut chip thickness. However, when the wavy tool path between successive workpiece revolutions is out of phase (Fig. 1c,1d), the uncut chip thickness will vary periodically during cutting. If the modulation amplitude is sufficiently high (Fig. 1d), the wavy tool path between successive revolutions will intercept, leading to the tool being periodically disengaged from the workpiece. In this case, the continuous cutting transforms into discrete cutting which is the desired MAM process.

The modulation amplitude required for realizing discrete cutting or effective MAM depends on the tool feed per revolution (h_0) and the phase shift (ϕ) of the wavy tool path between successive revolutions as: [18]

$$\frac{A}{h_0} \geq \frac{1}{2sin(\phi/2)} \tag{1}$$

The phase shift ϕ is determined by the modulation frequency to rotation frequency ratio, or simply referred to as the frequency ratio (f_m/f_w), as: [18]

$$\phi = 2\pi\left(\frac{f_m}{f_w} - INT\left[\frac{f_m}{f_w}\right]\right),\ 0 \leq \phi \leq 2\pi \tag{2}$$

where INT[] denotes the integer part of the modulation ratio. Therefore, ϕ is merely determined by the fractional part of the frequency ratio.

Based on Eqs. 1 and 2, the threshold amplitude to the feed per revolution ratio (A/h_0) for achieving discrete cutting can be depicted as a single U-shaped curve as a function of ϕ (Fig. 2a) or depicted as a series of U-shaped curves as a function of the frequency ratio f_m/f_w (Fig. 2b). Clearly, the threshold amplitude is the lowest when $\phi = \pi$ or f_m/f_w is at a half value between the integers, i.e., 0.5, 1.5, 2.5, etc. These points correspond to the bottom location of each U-curve where the threshold amplitude is only half of the feed per revolution ($A = 0.5h_0$). Other phase shifts or frequency ratios will result in higher threshold amplitude. When the frequency ratio is at integer values corresponding to $\phi = 0$ or 2π (see Fig. 1b), the threshold amplitude is approaching infinity. In other words, it is theoretically impossible to achieve discrete cutting at these frequency ratios. From the control point of view, varying the integer part of the frequency ratio is to change from one U-curve to another U-curve, and varying the fractional part of the frequency ratio is to change the phase shift within the same U-curve. A good modulation system should offer a wide range of modulation conditions covering a sufficient number of U-curves with the ability to accurately control the modulation frequency and amplitude.

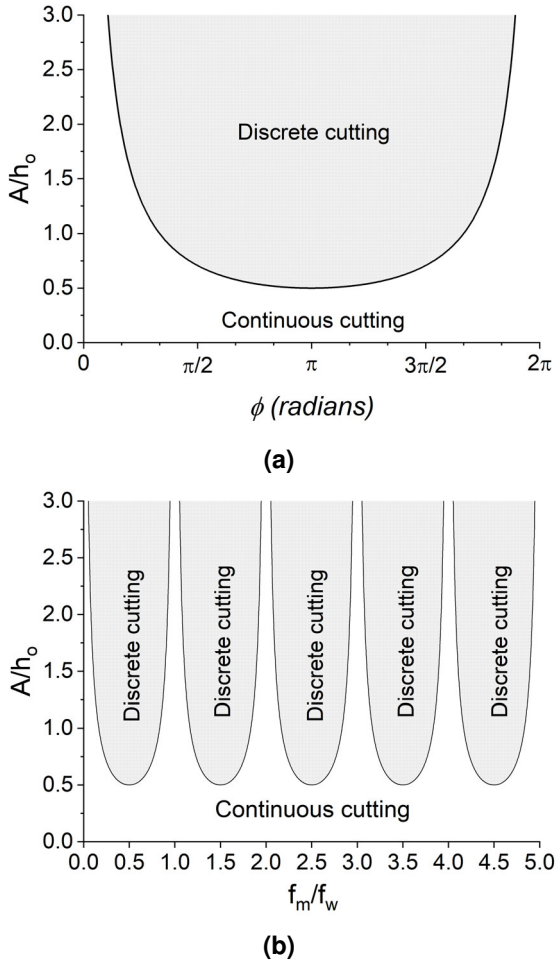

Fig. 2: The discrete cutting regimes demarcated by U-shaped curve of the threshold amplitude ratio as a function of (a) phase shift and (b) frequency ratio.

3. Modulated Orthogonal Cutting Setup

A simple modulation system realized by piezo stack actuation and linear guide coupling was designed and constructed (Fig. 3). The modulation system includes (1) a stationary frame, (2) a moving stage, (3) a linear guide/rail system, and (4) a piezo stack actuator. The casing of the piezo actuator was fixed with the vertical section of the stationary frame. The actuator head was rigidly connected to the back of the moving stage using a screw connection. The bottom of the moving stage was connected with the horizontal section of the stationary frame through the linear guide/rail system. The tool holder was fixed on the moving stage using a screw connection. Under the actuation of the piezo stack, the tool holder, moving stage, and linear guide will vibrate as a single rigid mass. The vibrating mass of the current system was measured to be 0.85 kg. The piezo ac-

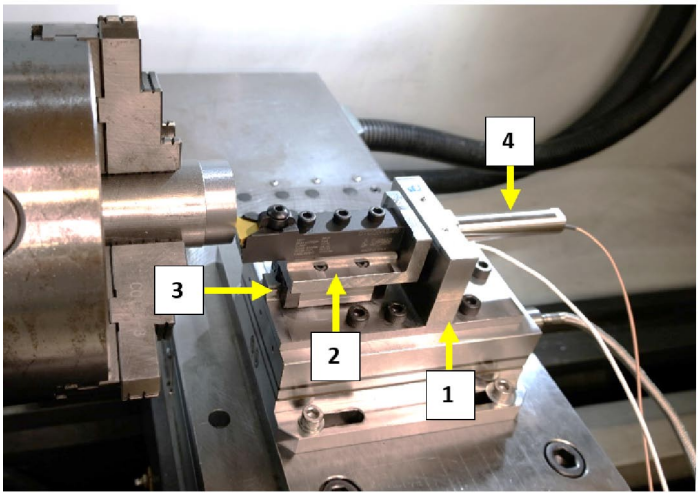

Fig. 3: Modulated orthogonal cutting setup.

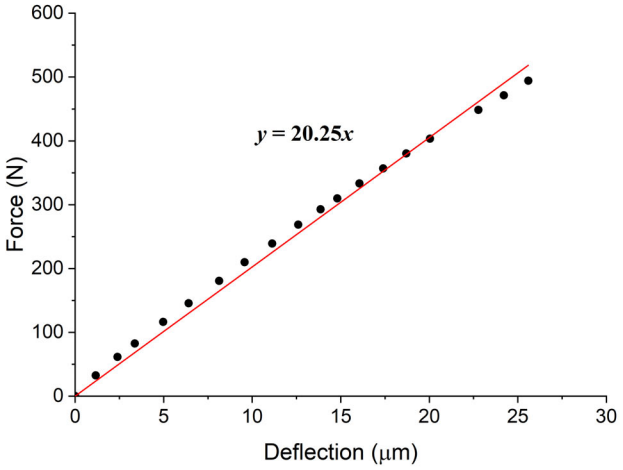

Fig. 4: Force versus deflection during quasi-static loading of the device assembly in the feed direction.

tuator has a nominal stroke of 100 μm which requires a driving voltage of up to 150 V. The maximum force generation from the actuator is 3500 N. The frequency and amplitude of the tool vibration were controlled by controlling the sinusoidal voltage input to the piezo actuator. A waveform generator (BK4007B) and a power amplifier (MMech PX200) were used to produce the sinusoidal voltage at the desired frequency and amplitude.

To measure the forces imposed on the modulation device, the stationary frame was mounted on a 3-component dynamometer (Kistler 9257B). To measure the vibration displacement of the tool holder and the moving stage, a capacitance displacement sensor probe was installed through a hole in the vertical section of the stationary frame and was facing the back wall of the moving stage. The force and displacement signals were recorded using a data acquisition system (National Instrument 6361) at 5000 samples per second and processed with a low-pass filter with a cut-off frequency of 500 Hz.

The modulation device assembly was installed on the carriage of a Haas TL-1 toolroom lathe to conduct orthogonal tube turning experiments (Fig. 3). The workpiece material was AISI 1045 steel. The wall thickness and the outer diameter of the tube were 1.5 mm and 50-52 mm, respectively. Uniformity of the wall thickness and concentricity with the spindle axis was ensured by a finishing boring of 15 mm length of the tube prior to the experiment. The cutting tool used was a TPG433 TiN coated carbide insert. After installing on the tool holder, the rake and relief angles of the tool were 0° and 11°, respectively.

4. Calibration of Modulation System

Before conducting the turning experiments, the modulation system was calibrated by two simple tests. In the first test, the device assembly was quasi-statically loaded in the axial (feed) direction while the tool vibration was turned off. This was done by slowly moving the lathe carriage to engage the cutting tool with the workpiece which was held stationary (not rotating). Figure 4 shows the measured force versus the deflection measured at the back of the moving stage during the tool-workpiece engagement. It can be seen that the generated deflection is linearly proportionate to the applied force in the axial direction. The axial stiffness of the device assembly is reflected by the slope of the linear curve fitting, which is 20.25 N/μm.

In the second test, the tool vibration was turned on by various sinusoidal voltage inputs while the device assembly was not loaded. The actuated vibration displacement was measured by the displacement sensor. The tool vibration was correlated with the sinusoidal voltage signals. Figure 5 shows the applied voltage signals and the resulting tool vibrations at two frequencies. It can be observed that the vibration followed the voltage signal closely in the sinusoidal form. There is no phase shift between the voltage signal and the generated tool vibration. Therefore, the vibration frequency was the same as the frequency of the applied voltage signal.

Furthermore, the amplitude of the generated vibration was linearly dependent on the amplitude of the voltage signal. Figure 6 shows the peak-to-peak vibration amplitude (A_{pp}) plotted against the applied peak-to-peak voltage amplitude (V_{pp}) at three different frequencies. The linear relationship between the vibration amplitude and the voltage amplitude was basically the same for different frequencies. This indicates that the vibration amplitude is independent of the frequency. This becomes more evident in Fig. 7, where the peak-to-peak vibration amplitude at the maximum voltage (V_{pp} = 150 V) is plotted for different frequencies ranging from 10 to 120 Hz. It can be seen that the vibration amplitude (A_{pp}) remained essentially the same at about 95 μm in the frequency range tested. These results indicate that the frequency and amplitude of the tool vibration can be controlled independently by controlling the frequency and amplitude of the voltage signal, respectively.

5. Orthogonal Cutting Experiments

The modulation system was used to conduct orthogonal tube turning on AISI 1045 steel at various cutting and modulation

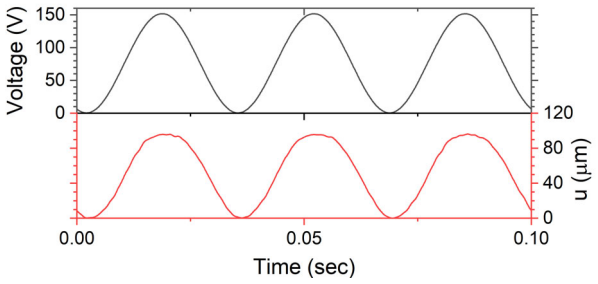

(a) f_m = 30 Hz

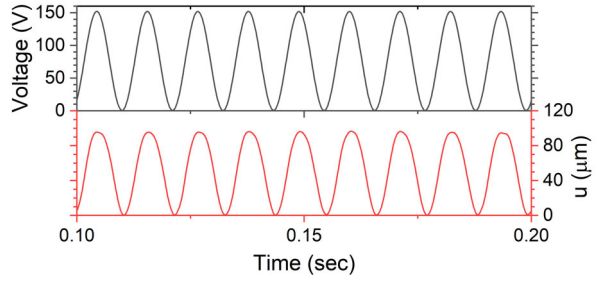

(b) f_m = 90 Hz

Fig. 5: The corresponding sinusoidal voltage inputs and generated tool vibration displacements at two frequencies.

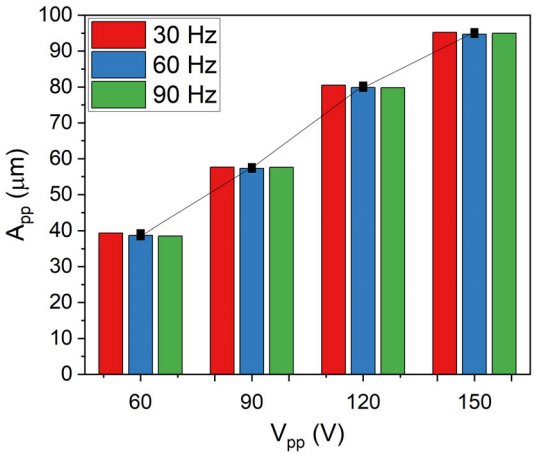

Fig. 6: The vibration amplitude (A_{pp}) calibrated at different voltage amplitudes (V_{pp}) and frequencies.

conditions. For all modulation conditions, the driving voltage was always controlled at a peak-to-peak amplitude of 150 V which utilized the full stroke of the piezo stack to actuate the tool vibration.

5.1. Tests by varying frequency ratio

In the first set of tests, the frequency ratio and phase shift were varied while the cutting speed and feed rate were fixed at v_c = 60 m/min and h_0 = 0.06 mm/rev, respectively. Figure 8 shows the measured forces (F_c in the cutting direction and F_f in the feed direction) and the vibration displacement (u) during one spindle revolution for three frequency ratios. The three frequency ratios had the same integer part but differed in their fractional part, so they belonged to the same U-curve but resulted in three different phase shifts. It can be seen in all cases, the forces varied in a steady manner following closely the vibration cycle. The forces periodically reached zero indicating the disengagement of the tool from the workpiece. The duration of the tool-work disengagement within a vibration cycle increases as ϕ changes from $\pi/2$ to $2\pi/3$, and further to π. This is because the actual applied amplitude ratios (A/h_0) for the three ϕ were 0.72, 0.68, and 0.72, respectively (with A measured from vibration displacement), while the threshold amplitude ratios were 0.71, 0.57, and 0.5, respectively (per Eq. 1). At $\phi = \pi/2$, the applied amplitude exceeded the threshold by a small amount, while at $\phi = \pi$, the applied amplitude exceeded the threshold by a large margin, resulting in a longer tool-work disengagement duration. It can also be observed that the force cycles had sharp peaks at $\phi = \pi/2$ and $2\pi/3$, while the force cycles had flat peaks at $\phi = \pi$. The peak force was noticeably higher at $\phi = 2\pi/3$ compared to $\phi = \pi/2$ and π. For comparison, the measured F_c and F_f in CM were nearly constant at 194 N and 93 N, respectively, for the same cutting speed and feed rate.

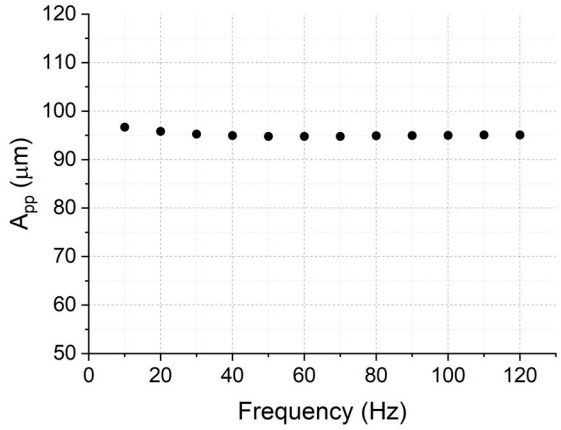

Fig. 7: The vibration amplitude (A_{pp}) calibrated at different frequencies for V_{pp} = 150 V.

Figure 9 shows the uncut chip thickness variation during one vibration cycle for the three ϕ, which was calculated from the tool path based on the corresponding cutting and modulation conditions. It can be noted that the variation in forces (Fig. 8) closely resembles the variation in the uncut chip thickness (Fig. 9). This means that the force variation in modulated cutting is mainly caused by the variation in uncut chip thickness during the process.

The cutting forces can be related to the uncut chip thickness by a simple mechanistic force model as [19]:

$$\begin{aligned} F_c &= K_{cs} bh + K_{ce} b \\ F_f &= K_{fs} bh + K_{fe} b \end{aligned} \tag{3}$$

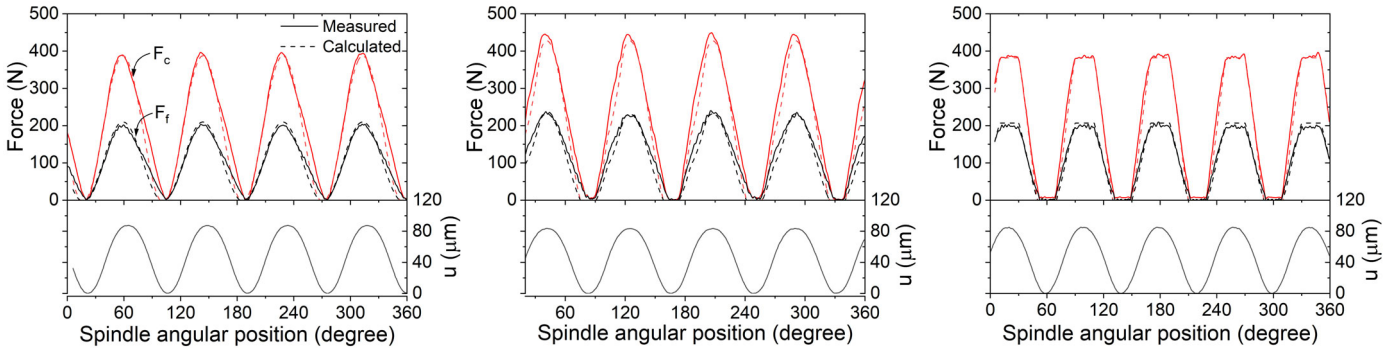

(a) $\phi = \pi/2$, $f_m/f_w = 4.25$, f_m=25.5 Hz **(b)** $\phi = 2\pi/3$, $f_m/f_w = 4.33$, f_m =26 Hz **(c)** $\phi = \pi$, $f_m/f_w = 4.5$, f_m = 27 Hz

Fig. 8: Forces and vibration displacements for different phase shifts at v_c = 60 m/min and h_0 = 0.06 mm/rev.

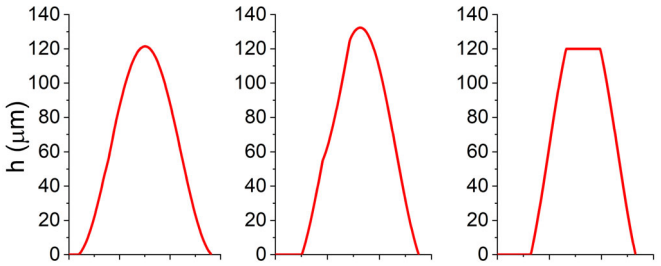

(a) $\phi = \pi/2$ **(b)** $\phi = 2\pi/3$ **(c)** $\phi = \pi$

Fig. 9: The variation of uncut chip thickness during one vibration cycle determined analytically for the three conditions corresponding to Fig. 8.

Table 1: Experimentally determined cutting force coefficients.

Force coefficients	Values
K_{cs}	2043.2 [N/mm^2]
K_{ce}	15.6 [N/mm]
K_{fs}	1149.8 [N/mm^2]
K_{fe}	2.6 [N/mm]

where h is the uncut chip thickness and b is the width of the cut. K_{cs} and K_{fs} are the force coefficients related to shearing for the primary cutting force and feed force, respectively. K_{ce} and K_{fe} are the force coefficients related to the plowing at the tool edge. These force coefficients can be determined by conducting conventional orthogonal cutting at various feed rates. Table 1 lists the experimentally determined force coefficients for cutting AISI 1045 steel at the speed of v_c = 60 m/min.

Using the mechanistic force model described by Eq. 3 and the uncut chip thickness variations shown in Fig. 9, the forces during modulated cutting were calculated and shown by the dashed profiles in Fig. 8. The calculated forces were in good agreement with the measured forces at all three phase shifts.

Figure 10 shows the forces and vibration displacement during one spindle revolution for three frequency ratios where only the integer part of the frequency ratio was varied. The three frequency ratios belong to three different U-curves but result in the same phase shift ($\phi = \pi$). It can be observed that the vibration remained well in the sinusoidal form as the frequency increased up to 56.8 Hz. Furthermore, the force variation during each vibration cycle and the peak force was generally the same for the three frequency ratios. This is because the same phase shift leads to the same variation of uncut chip thickness during each vibration cycle. The increase in the integer part of the frequency ratio just leads to the same force variation cycle occurring faster; there are effectively more vibration cycles during one spindle revolution. The forces calculated based on Eq. 3 and the uncut chip thickness variation again agree reasonably well with the measured forces for all three frequency ratios. These results also demonstrate the good control ability and robustness of the modulation system in conducting modulated cutting.

5.2. *Tests by varying feed rate and speed*

In the second set of tests, the cutting parameters (feed rate and speed) were varied while the frequency ratio was fixed at 4.5 and the peak-to-peak voltage amplitude was fixed at 150 V. Figure 11 shows the measured forces for three feed rates (h_0 = 0.04, 0.06, and 0.08 mm/rev) at the cutting speed of v_c = 90 m/min. Based on the same applied frequency ratio, the threshold peak-to-peak vibration amplitude (A_{pp}) is 0.04, 0.06, and 0.08 mm for the three feed rates. The actually applied A_{pp} was slightly larger than 0.08 mm, so discrete cutting was realized for all three feed rates. This is evident by the fact that the measured forces periodically reached zero. However, as the feed rate increases, the margin by which the applied vibration amplitude exceeded the threshold amplitude decreases, which leads to a decrease in the duration of tool disengagement. It is observed the peak force during each vibration cycle increases with the feed rate. This is because the maximum uncut chip thickness increases with the feed rate.

Figure 12 shows the measured forces for three cutting speeds (v_c = 60, 90, 120 m/min) at the same feed rate (h_0 = 0.06

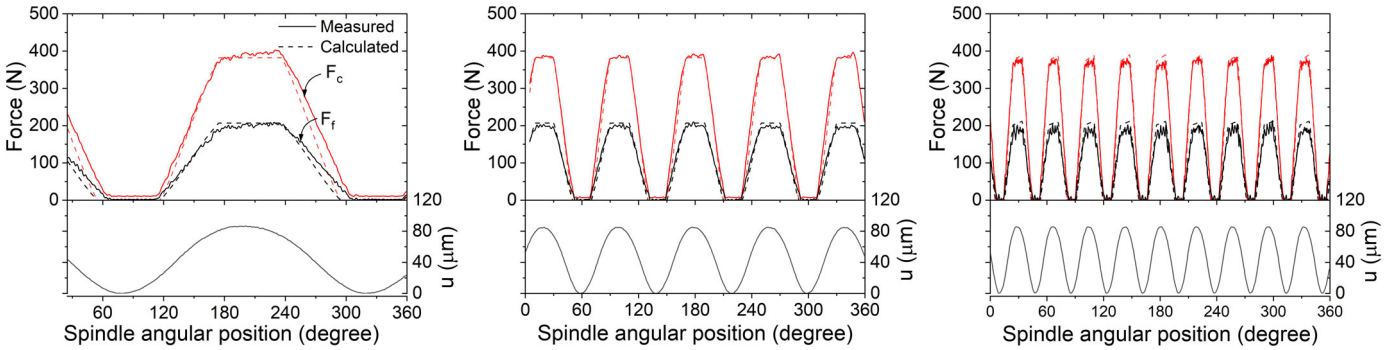

(a) $f_m/f_w = 1.5$, $f_m = 9$ Hz **(b)** $f_m/f_w = 4.5$, $f_m = 27$ Hz **(c)** $f_m/f_w = 9.5$, $f_m = 56.8$ Hz

Fig. 10: Forces and vibration displacements for different frequency ratios with same phase shift at $v_c = 60$ m/min, $h_0 = 0.06$ mm/rev.

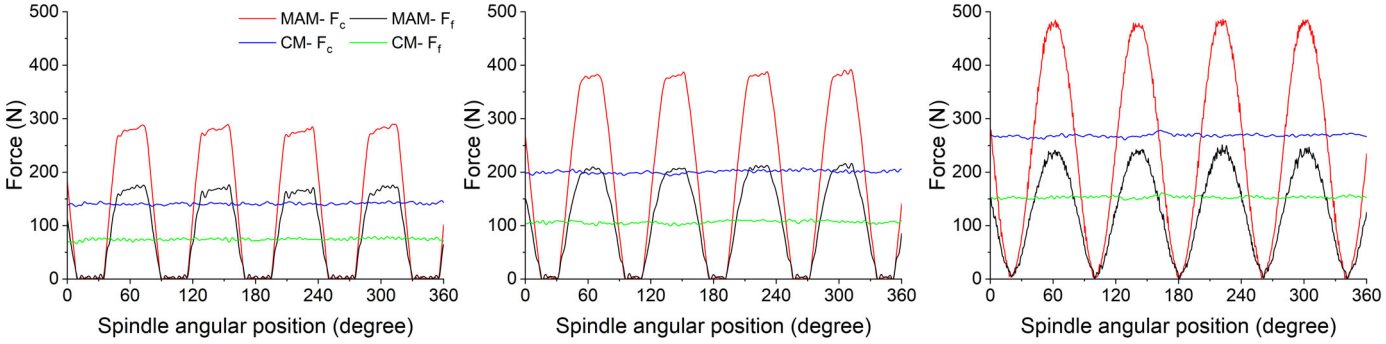

(a) $h_0 = 0.04$ mm/rev **(b)** $h_0 = 0.06$ mm/rev **(c)** $h_0 = 0.08$ mm/rev

Fig. 11: Measured forces for different feed rates at $f_m/f_w = 4.5$ and $v_c = 90$ m/min.

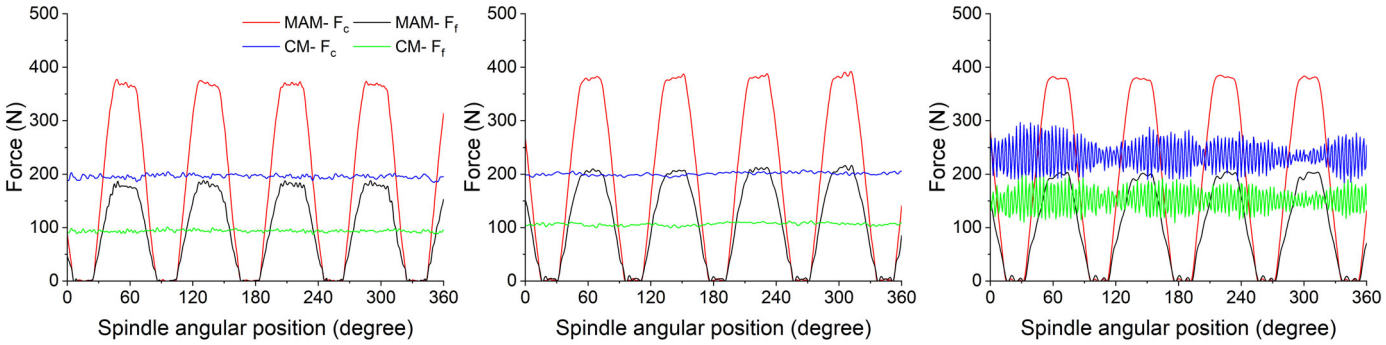

(a) $v_c = 60$ m/min, $f_m = 27$ Hz **(b)** $v_c = 90$ m/min, $f_m = 40.5$ Hz **(c)** $v_c = 120$ m/min, $f_m = 55.8$ Hz

Fig. 12: Measured forces for different cutting speeds at $f_m/f_w = 4.5$ and $h_0 = 0.06$ mm/rev.

mm/rev). To maintain the same frequency ratio for the three speeds, the vibration frequency has to be increased proportionally with the workpiece rotational frequency. Force variation during modulated cutting remains unchanged with cutting speed because frequency ratio and feed rate were constant, resulting in the same uncut chip thickness variation in each vibration cycle. Forces continue to be primarily influenced by uncut chip thickness.

It can also be observed that chatter vibration occurred during conventional cutting at the speed of $v_c = 120$ m/min, but it did not occur during modulated cutting at the same speed. This indicates that modulated cutting has the capability to suppress chatter and increase the dynamic stability of the cutting process.

Table 2: Comparison of calculated and measured vibration amplitudes for all modulated cutting tests.

v_c (m/min)	f_m/f_w	ϕ	h_0 (mm/rev)	f_m (Hz)	Measured amplitude A_{pp} (μm)	Calculated amplitude A_{pp} (μm)	% Error
60	1.5	π	0.06	9	86.64	85.58	1.22
60	4.25	$\pi/2$	0.06	25.5	86.98	85.57	1.62
60	4.33	$2\pi/3$	0.06	26	83.44	83.61	0.2
60	4.5	π	0.06	27	86.18	85.73	0.52
60	9.5	π	0.06	56.8	85.12	85.60	0.57
90	4.5	π	0.04	40.5	86.41	86.39	0.02
90	4.5	π	0.06	40.5	83.99	84.60	0.73
90	4.5	π	0.08	40.5	82.77	82.63	0.17
120	4.5	π	0.06	55.8	83.4	84.99	1.91

5.3. Amplitude reduction

In all modulated cutting tests, it was found that the vibration amplitude during cutting was always smaller than the calibrated amplitude when the device assembly was not loaded. The calibrated A_{pp} at V_{pp} = 150 V was about 95 μm (Fig. 7). Table 2 lists all modulated cutting tests and the measured A_{pp}. The measured A_{pp} values range from 82−87 μm which are all below the calibrated value of 95 μm. The reduction in vibration amplitude is caused by the finite stiffness of the device assembly in the actuation (or feed) direction. Under the variable feed force during modulated cutting, the device assembly also undergoes variable elastic deformation in the actuation direction. This leads to the reduction of vibration amplitude. Therefore, the amplitude reduction ΔA_{pp} can be calculated as:

$$\Delta A_{pp} = F_{max}/k \tag{4}$$

where F_{max} is the feed force corresponding to the peak displacement in a vibration cycle and k is the stiffness of the device assembly which was determined to be 20.25 N/μm (see Fig. 4). Using Eq. 4 and the calibrated amplitude under the no-load condition, the reduced vibration amplitude during modulated cutting can be calculated. The calculated values of A_{pp} are also listed in Table 2. It can be seen that the calculated values are in good agreement with the measured values as the error is within 2% for all cases.

6. Summary

In this study, a modulated orthogonal cutting setup was realized by piezo stack actuation and linear guide coupling. The modulation system was evaluated by conducting orthogonal tube turning tests on AISI 1045 steel, and measuring the forces and vibration displacements during the test for various cutting and modulation conditions. The results demonstrate that the modulation system is able to accurately control the frequency and amplitude of the tool vibration to achieve desired frequency ratio f_m/f_w, phase shift ϕ, and amplitude ratio A/h_0 for a good range of practical cutting speeds and feeds.

The force variation during modulated cutting is mainly caused by the variation in the uncut chip thickness during each tool vibration cycle which is determined by the phase shift ϕ. The mechanistic model based on experimentally determined force coefficients and theoretically determined uncut chip thickness can be used to calculate the forces for given modulation conditions, which are found to be in good agreement with the measured forces.

The modulation device assembly has finite stiffness. The elastic deformation under the variable forces in the actuation (feed) direction results in the reduction in vibration amplitude during modulated cutting. However, the actual vibration amplitude during cutting can be calculated based on the measured feed force and the stiffness of the device assembly, which are found to be in good agreement with the measured vibration amplitude.

Acknowledgements

This work was supported by National Science Foundation CMMI grant no. 2019320.

References

[1] Yang Guo and James B. Mann. Control of chip formation and improved chip ejection in drilling with modulation-assisted machining. *Journal of Manufacturing Science and Engineering, Transactions of the ASME*, 142, 7 2020.

[2] J B Mann, C J Saldana, Y Guo, H Yeung, W D Compton, and S Chandrasekar. Effects of controlled modulation on surface textures in deep-hole drilling. *SAE International Journal of Materials and Manufacturing*, 6(1):24–32, 2013.

[3] Wilfredo Moscoso, Efe Olgun, W. Dale Compton, and Srinivasan Chandrasekar. Effect of low-frequency modulation on lubrication of chip-tool interface in machining. *Journal of Tribology*, 127:238–244, 1 2005.

[4] Yang Guo, Tyler Stalbaum, James Mann, Ho Yeung, and Srinivasan Chandrasekar. Modulation-assisted high speed machining of compacted

graphite iron (cgi). *Journal of Manufacturing Processes*, 15:426–431, 10 2013.

[5] Soohyun Nam, Bora Eren, Takehiro Hayasaka, Burak Sencer, and Eiji Shamoto. Analytical prediction of chatter stability for modulated turning. *International Journal of Machine Tools and Manufacture*, 165:103739, 6 2021.

[6] Yo Kamada, Ayako Kitakaze, Kazuhiko Sannomiya, Takaichi Nakaya, and Hiroyuki Sasahara. Mechanism to suppress regenerative chatter vibration due to the effect of air-cutting and multiple regeneration during low frequency vibration cutting. *Precision Engineering*, 78:1–18, 11 2022.

[7] Kiyoshi Okamura, Hiroyuki Sasahara, Toshiaki Segawa, and Masaomi Tsutsumi. Low-frequency vibration drilling of titanium alloy. *JSME International Journal Series C Mechanical Systems, Machine Elements and Manufacturing*, 49:76–82, 9 2006.

[8] P. N. Chhabra, B. Ackroyd, W. D. Compton, and S. Chandrasekar. Low-frequency modulation-assisted drilling using linear drives. *http://dx.doi.org/10.1243/0954405021519997*, 216:321–330, 12 2005.

[9] A. Sadek, M. H. Attia, M. Meshreki, and B. Shi. Characterization and optimization of vibration-assisted drilling of fibre reinforced epoxy laminates. *CIRP Annals*, 62:91–94, 1 2013.

[10] Nicolas Guibert, Henri Paris, and Joël Rech. A numerical simulator to predict the dynamical behavior of the self-vibratory drilling head. *International Journal of Machine Tools and Manufacture*, 48:644–655, 5 2008.

[11] Jérémy Jallageas, Jean Yves K Nevez, Mehdi Chérif, and Olivier Cahuc. Modeling and optimization of vibration-assisted drilling on positive feed drilling unit. *The International Journal of Advanced Manufacturing Technology 2012 67:5*, 67:1205–1216, 10 2012.

[12] H. G. Toews, W. D. Compton, and S. Chandrasekar. A study of the influence of superimposed low-frequency modulation on the drilling process. *Precision Engineering*, 22:1–9, 1 1998.

[13] Ryan Copenhaver, Mark A. Rubeo, Steven Guzorek, Saurabh Landge, K. Scott Smith, John Ziegert, and Tony L. Schmitz. A fundamental investigation of modulated tool path turning mechanics. *Procedia Manufacturing*, 10:159–170, 1 2017.

[14] Akihito Miyake, Hiroyuki Sasahara, Ayako Kitakaze, Seiko Katoh, Masahiro Muramatsu, Kenji Noguchi, Kazuhiko Sannomiya, and Takaichi Nakaya. Effect of low frequency vibration applied to feed direction on turning process. *International Symposium on Flexible Automation, ISFA 2016*, pages 356–358, 12 2016.

[15] Bora Eren and Burak Sencer. Mechanistic cutting force model and specific cutting energy prediction for modulation assisted machining. *Procedia Manufacturing*, 48:474–484, 1 2020.

[16] Yuan Gao, Ronglei Sun, Yanni Chen, and Jürgen Leopold. Analysis of chip morphology and surface topography in modulation assisted machining. *International Journal of Mechanical Sciences*, 111-112:88–100, 6 2016.

[17] Juan Sandoval, Aaqib Ali, Patrick Kwon, and Yang Guo. Modulation-assisted machining of compacted graphite iron with coated carbide tool in dry condition. *Manufacturing Letters*, 33:452–460, 9 2022.

[18] J. B. Mann, Y. Guo, C. Saldana, W. D. Compton, and S. Chandrasekar. Enhancing material removal processes using modulation-assisted machining. *Tribology International*, 44:1225–1235, 9 2011.

[19] Yusuf Altintas. *Manufacturing Automation*. Cambridge University Press, 1 2012.